Parameter Identification and Maximum Power Estimation of Battery/Supercapacitor Hybrid Energy Storage System Based on Cramer–Rao Bound Analysis

Ziyou Song, *Member, IEEE*, Jun Hou, *Student Member, IEEE*, Heath F. Hofmann, *Senior Member, IEEE*, Xinfan Lin, *Member, IEEE*, and Jing Sun, *Fellow, IEEE*

***Abstract*—This paper presents the analysis, design, and experimental validation of parameter identification of battery/supercapacitor (SC) hybrid energy storage system (HESS) for the purpose of condition monitoring and maximum power estimation. The analytic bounds on the error of battery and SC parameter identification, considering voltage measurement noise, are obtained based on the Fisher information matrix and Cramer–Rao bound analysis. The identification of different parameters requires different signal patterns to ensure high accuracy, rendering tradeoffs in the multiparameter identification process. With an appropriately designed current profile, HESS parameters are identified using recursive least squares with a forgetting factor. The identified parameters are then used to estimate the maximum power capability of the HESS. The maximum power capabilities of the battery and SC are estimated for both 1 and 30 s time horizons. The parameter identification algorithm can be applied to systems including either batteries or SCs when the optimal excitation current can be injected. Experimental validation is conducted on an HESS test-bed, which shows that the proposed algorithm is effective in estimating the HESS maximum power based on appropriate current excitation.**

***Index Terms*—Cramer–Rao (CR) bound, hybrid energy storage system (HESS), identification accuracy, maximum power estimation, parameter identification, recursive least square (RLS).**

Manuscript received March 28, 2018; revised June 18, 2018; accepted July 18, 2018. Date of publication July 23, 2018; date of current version March 29, 2019. This work was supported in part by the National Science Foundation under Grant CNS 1329539, and in part by the U.S. Office of Naval Research under Grant N00014-16-1-3108. Recommended for publication by Associate Editor G. Oriti. *(Corresponding author: Jun Hou.)*

Z. Song is with the Department of Electric Engineering and Computer Science and the Department of Naval Architecture and Marine Engineering, University of Michigan, Ann Arbor, MI 48109 USA (e-mail:

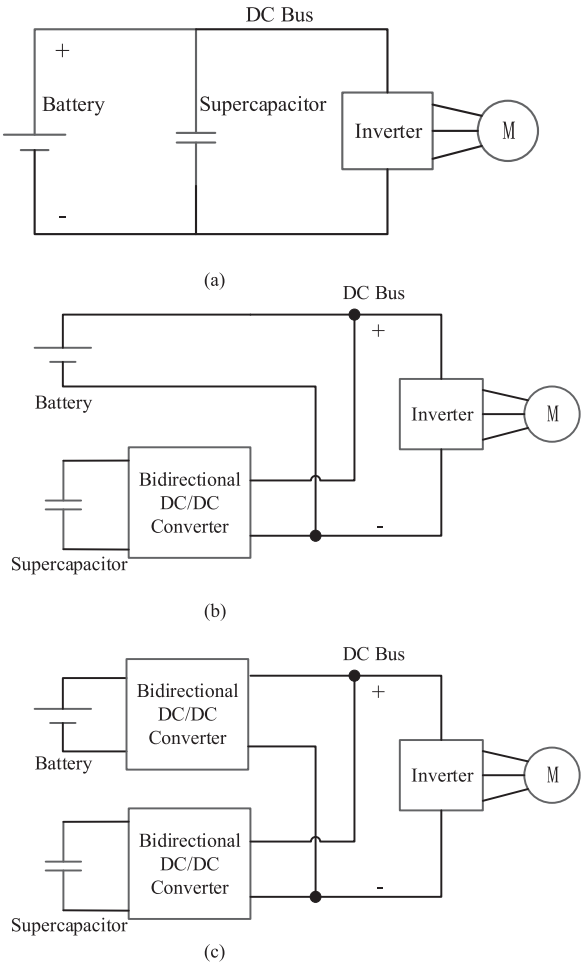

Fig. 1. Three typical HESS topologies. (a) Passive HESS topology. (b) Semiactive HESS topology. (c) Fully active HESS topology.

Commonly used algorithms include Kalman filters [16], least-squares-based methods [17], moving-horizon observers [18], and gradient-based algorithms [13].

Although the identification algorithm is important, signals used in the identification process also significantly influence the identification accuracy [19]. For example, no parameter can be identified when both battery and SC currents are constant. In general, assuming an appropriate identification algorithm is used, the persistently exciting condition should be satisfied to guarantee identification convergence [20]. In addition, most algorithms consider the data indiscriminately regardless of the information richness in terms of the parameters to be identified. It has been established that the identification accuracy can be impaired when insufficiently rich data is adopted [21], thus providing a guideline on data selection based on the fundamental relationship between the estimation accuracy and the measurement data. In addition, Lin and Stefanopoulou analyzed the influence of data on the combined estimation of battery SoC, capacity, and ohmic resistance [19]. Similarly, Rothenberger *et al.* optimized battery test data to maximize the Fisher information matrix (an identifiability metric) for a second-order dynamic ECM of a lithium ion battery [22]. Klintberg *et al.* used Cramer–Rao (CR) lower bounds to quantify the accuracy of Bayesian estimators, which were applied to a second-order nonlinear ECM of a lithium battery [23]. SoC estimation error considering sensor bias [24], models, and algorithms are also investigated [25]. More and more studies focus on the analysis and optimization of the battery parameter identification accuracy, but the optimal current cannot be directly adopted in the battery-only configuration. The persistently exciting requirement can be in conflict with the desired operational goals of the system. The HESS, which is inherently an overactuated system, offers an additional degree of freedom to generate excitation currents for battery/SC currents in order to achieve a better parameter identification performance. Without perturbing the power supply function, the rich information for learning the system can be provided rather than passively collecting signals.

This paper presents an analytic evaluation of data-dependent estimation accuracy based on the Fisher information matrix and CR bound analysis using the framework formulated in [22]. It shows that there is an inherent tradeoff associated with identifying all parameters of an HESS simultaneously when signals are corrupted by noise. In addition, a guideline on designing current profiles for battery and SC to properly identify different parameters simultaneously is provided. Based on the analysis, a current profile is designed to excite the battery pack, and the excitation for SC can be automatically generated by the bus voltage controller. Experimental results show that the identification performance is satisfactory when the data is appropriately designed. Based on the identification results, the maximum discharge/charge power capability of the HESS, which is one of the most important boundary conditions in EMSs, is estimated [26]. The maximum power capability of the battery is constrained by its voltage, current, and SoC [27], while the maximum power of the SC is constrained by current and voltage limits [28]. Since the maximum power is calculated based on the ECMs of battery and SC, so the maximum power also depends upon accurate ECM parameters. In addition, the maximum power of the dc/dc converter is limited by the voltage and current ratings of its electronic components [29], [30]. The maximum power of HESS can, therefore, be determined by considering all these limitations simultaneously, if relevant parameters can be accurately estimated. It has been proven that the HESS can significantly boost peak power capacity and reduce power loss when compared to the battery-only system, while the system volume and weight are minimally impacted [5].

This paper is organized as follows: In Section II, ECMs of the battery and SC are introduced. CR bounds of the target parameters are derived. Section III presents the maximum power estimation process for the HESS. In Section IV, experimental results are provided, which validate the effectiveness of the approach. The results of maximum power estimation are also presented. Conclusions are drawn in Section V.

II. CR Bounds of the Target Parameters

A. Battery Model

An accurate battery model is needed to achieve a reliable battery state estimation [31]. The ECM adopted in this paper is shown in Fig. 2, where an ohmic resistor with resistance R_s, a

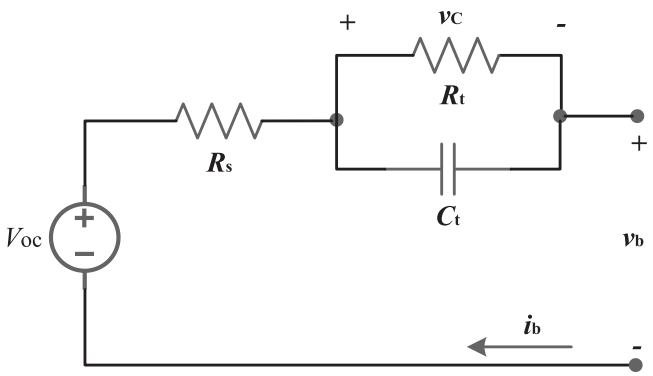

Fig. 2. ECM of a battery.

parallel RC network $(R_t//C_t)$, and a dc source with voltage $V_{\rm oc}$ are connected in series [32]. It has been shown that the first-order RC model is adequate and convenient for many applications [14], especially for system-level EMS development.

The battery terminal voltage and current are defined as v_b and i_b, respectively (positive i_b for discharge and negative i_b for charge). According to Kirchhoff's laws, the ECM dynamics can be presented as

$$\begin{cases} \dot{v}_C = -\frac{1}{C_t R_t} v_C + \frac{1}{C_t} i_b \\ v_b = V_{\rm OC} - R_s i_b - v_C \end{cases} \tag{1}$$

where v_C is the voltage across the RC network, as shown in Fig. 2, and cannot be measured in experiments. $V_{\rm OC}$ and R_s are functions of battery SoC and their variations with respect to time are much smaller than that of v_C [33]. Thus, $V_{\rm OC}$ and R_s in (1) can be assumed to be constant, and the time derivative of v_b can be obtained as follows:

$$\dot{v}_b \approx -\frac{1}{\tau} v_b - R_s \dot{i}_b - \frac{R_t + R_s}{\tau} i_b + \frac{1}{\tau} V_{\rm OC} \tag{2}$$

where $\tau = R_t C_t$. $\dot{i}_b$ can be carefully computed by the filtered differentiating i_b, which can be measured in practical applications. To estimate the battery maximum power, the battery ECM parameters, including R_s, R_t, τ, and $V_{\rm OC}$, should be constantly identified since they vary with operating conditions (e.g., battery SoC and temperature) and battery health degradation [34]. Based on (2), the parametric model of the battery can be expressed as

$$\dot{v}_b = {\theta_{\mathbf{b}}}^T \mathbf{x_b} \tag{3}$$

where

$$\begin{cases} \theta_{\mathbf{b}} = \left[R_s \quad \frac{R_t + R_s}{\tau} \quad \frac{1}{\tau} \quad \frac{V_{\rm OC}}{\tau} \right]^T \\ \mathbf{x_b} = \left[-\dot{i}_b \quad -i_b \quad -v_b \quad 1 \right]^T. \end{cases} \tag{4}$$

$\theta_{\mathbf{b}}$ is the parameter vector to be identified and $\mathbf{x_b}$ is the information vector that can be obtained through measurement and calculation. To provide sufficient theoretical background, $\mathbf{x}_b$ should be persistently exciting to ensure parameter convergence regardless of the algorithm used (e.g., extended Kalman filter, recursive least-squares (RLS) method, gradient-based method). This critical condition is important for parameter identification, and is assumed to be inherently satisfied by most existing literatures. To guarantee parameter convergence, at least two frequency components should be included in $\mathbf{x_b}$ because, for every two unknown parameters, one additional frequency component is required [20].

While persistent excitation is the basic requirement for convergence of estimation results, the accuracy of estimation further depends on the quality of the data. To further investigate the influence of the dataset on identification accuracy, the CR bound, which is the lower bound of the estimation error covariance of an unbiased estimation, is used in this paper to quantify the estimation accuracy [35]. The process for computing the time-averaged CR bound is introduced in the following. Assuming that the initial value of v_C is 0 and the initial value of v_b equals $V_{\rm OC}$, the Laplace transform of v_b can be derived based on (2) as

$$v_b(s) = \frac{1}{s} V_{\rm OC} - R_s i_{\rm b}(s) - \frac{R_t}{1+\tau s} i_b(s) \tag{5}$$

where s is the Laplace operator.

In order to evaluate the Fisher information matrix, the sensitivity of the measurement v_b to the target parameters are needed in the s-domain and they can then be expressed as

$$\begin{cases} \frac{\partial v_b}{\partial V_{\rm OC}}(s) = \frac{1}{s} \\ \frac{\partial v_b}{\partial R_s}(s) = -i_b(s) \\ \frac{\partial v_b}{\partial R_t}(s) = -\frac{1}{1+\tau s} i_b(s) \\ \frac{\partial v_b}{\partial \tau}(s) = \frac{R_t s}{(1+\tau s)^2} i_b(s). \end{cases} \tag{6}$$

Based on (6), the sensitivity of the measurement v_b to the target parameters in the time domain can be obtained through inverse Laplace transform L^{-1} as

$$\begin{cases} \frac{\partial v_b}{\partial V_{\rm OC}}(t) = {\rm L}^{-1}\left\{\frac{1}{s}\right\} \\ \frac{\partial v_b}{\partial R_s}(t) = {\rm L}^{-1}\left\{-i_b(s)\right\} \\ \frac{\partial v_b}{\partial R_t}(t) = {\rm L}^{-1}\left\{-\frac{1}{1+\tau s} i_b(s)\right\} \\ \frac{\partial v_b}{\partial \tau}(t) = {\rm L}^{-1}\left\{\frac{R_t s}{(1+\tau s)^2} i_b(s)\right\}. \end{cases} \tag{7}$$

Considering Gaussian noise in the v_b measurement, the symmetric time-average Fisher matrix $\bar{\mathbf{F}}_{\rm b}$ can, therefore, be calculated if $i_b(t)$ is a periodic waveform with period T as in (8) shown at the bottom of the next page, where σ_V^2 is the variance of the voltage measurement noise. The CR bounds, which represent the best achievable variance of the identification error for θ_i, can be obtained by inverting the Fisher matrix

$$\operatorname{cov}(\theta_i) \geq \underline{\sigma}^2(\theta_i) = \operatorname{diag}\left(\bar{\mathbf{F}}_b^{-1}\right)_i \tag{9}$$

where $\operatorname{cov}(\theta_i)$ is the variance of the identification error for parameter θ_i, $\underline{\sigma}^2(\theta_i)$ is the CR lower bound of θ_i, which represents the minimum achievable variance of the identification error for θ_i, and $\operatorname{diag}\left(\bar{\mathbf{F}}_b^{-1}\right)_i$ is the ith diagonal element of $\bar{\mathbf{F}}_b^{-1}$. The CR bound quantifies the estimation accuracy dictated by data, and a small CR bound indicates better identification accuracy. The general expression of the time-average Fisher matrix shown in (10) is complex in general. A current waveform that includes two frequency components is used to investigate its influence on

the CR bounds of identified parameters. To simplify the analysis, we assume two sinusoidal waveforms have the same amplitude. Let $i_{\rm b}(t)$ be

$$i_{\rm b}\left(t\right) = M\cos\left(\omega t\right) + M\cos\left(k\omega t\right) \tag{10}$$

where M is the current magnitude, ω is the current frequency, and k is a positive number $(k \neq 1)$. The excitation current can be expressed in the s-domain as

$$i_b\left(s\right) = \frac{Ms}{s^2+\omega^2} + \frac{Ms}{s^2+k^2\omega^2}. \tag{11}$$

In (7), the expressions of $\frac{\partial v_b}{\partial R_t}(t)$ and $\frac{\partial v_b}{\partial \tau}(t)$ include the exponential decay term $e^{-\frac{t}{\tau}}$, which converges to 0 as $t\to\infty$, based on the current in (10). The converged values of $\frac{\partial v_b}{\partial R_t}(t)$ and $\frac{\partial v_b}{\partial \tau}(t)$ as $t \to \infty$ are provided in [21]. Then, the CR bounds for $k = 2$, as an example, can be derived as (the integral interval $T = 2\pi/\omega$)

$$\begin{cases} \underline{\sigma}\left(V_{\rm OC}\right) = \sigma_V \\ \underline{\sigma}\left(R_s\right) = \frac{\sqrt{2}\sigma_V\sqrt{2+10\tau^2\omega^2+17\tau^4\omega^4}}{3M\tau^2\omega^2} \\ \underline{\sigma}\left(R_t\right) = \frac{2\sigma_V\sqrt{1+\tau^4\omega^4+16\tau^8\omega^8}}{3M\tau^2\omega^2} \\ \underline{\sigma}\left(\tau\right) = \frac{\sqrt{2}\sigma_V\sqrt{10+41\tau^2\omega^2+40\tau^4\omega^4}\left(1+5\tau^2\omega^2+4\tau^4\omega^4\right)}{3M\tau\omega^2 R_t\sqrt{2+16\tau^2\omega^2+20\tau^4\omega^4}}. \end{cases} \tag{12}$$

As shown in (12), the identification of $V_{\rm OC}$ is independent of the other parameters and current excitation can be increased to reduce the effects of measurement noise. Numerical analysis is presented to investigate the influence of ω on the CR bounds of R_s, R_t, and τ, as plotted in Fig. 2 for illustration. In the numerical analysis, the values of R_s, R_t, τ, M, and σ_V are set to be 60 mΩ, 200 mΩ, 60 s, 10 A, and 0.2 V, respectively. We point out that the parameter values in the numerical analysis are set based on *a priori* knowledge about the adopted battery pack. The rough values of the estimated parameters were obtained from the previous test. In addition, since the battery capacity is 100 Ah, we believe that a 10 A (i.e., 0.1 C-rate) current signal is acceptable.

As shown in Fig. 3, the CR bound of R_s monotonically decreases with frequency, which should be set as high as possible to improve the identification accuracy of R_s. As shown in Fig. 3(b), CR bounds of R_t and τ achieve their minimum values when the frequency is around 0.002 Hz (the frequencies for R_t and τ to achieve their minimum CR bounds are slightly different), and so the optimal frequency for R_t and τ identification is extremely low. It is seen that there is a tradeoff regarding the identification of R_s, R_t, and τ. In addition, the optimal frequency for R_t and τ identification will cause a long identification process, thus there is another tradeoff between identification accuracy and speed. A frequency around 0.004 Hz can be chosen as the theoretical optimal frequency to achieve a satisfactory identification performance. An analysis for $k = 5$ is also conducted and it has a slight difference with the result for $k = 2$. Both results show that a slow frequency component is needed to identify R_t and τ.

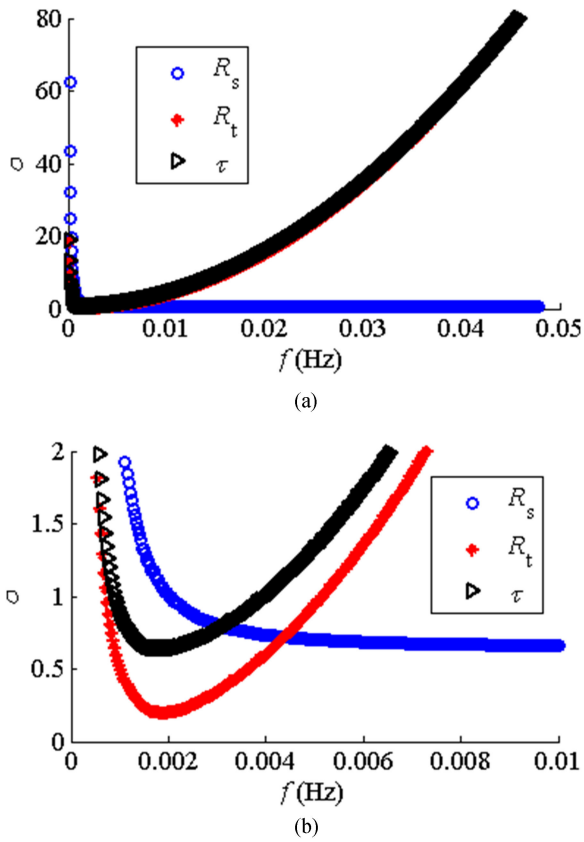

Fig. 3. CR bounds of R_s, R_t, and τ over frequency when $k = 2$. (a) CR bounds. (b) Zoom-in results.

The RLS with a forgetting factor will be used to iteratively identify the battery parameters based on (3). Detailed procedures of the RLS method are provided in [36]. Due to space limitations, the RLS is not further illustrated in this paper.

B. SC Model

The ECM shown in Fig. 4 has been verified to be effective to represent the real-time behavior of SCs at both high and low frequencies [15].

$$\bar{\boldsymbol{F}}_{\boldsymbol{b}} = \frac{1}{\sigma_V^2}\frac{1}{T}\begin{pmatrix} \int_0^T\left(\frac{\partial v_b}{\partial V_{\rm OC}}\right)^2 dt & \int_0^T \frac{\partial v_b}{\partial V_{\rm OC}}\frac{\partial v_b}{\partial R_s}dt & \int_0^T \frac{\partial v_b}{\partial V_{\rm OC}}\frac{\partial v_b}{\partial R_t}dt & \int_0^T \frac{\partial v_b}{\partial V_{\rm OC}}\frac{\partial v_b}{\partial \tau}dt \\ * * * & \int_0^T\left(\frac{\partial v_b}{\partial R_s}\right)^2 dt & \int_0^T \frac{\partial v_b}{\partial R_s}\frac{\partial v_b}{\partial R_t}dt & \int_0^T \frac{\partial v_b}{\partial R_s}\frac{\partial v_b}{\partial \tau}dt \\ * * * & * * * & \int_0^T\left(\frac{\partial v_b}{\partial R_t}\right)^2 dt & \int_0^T \frac{\partial v_b}{\partial R_t}\frac{\partial v_b}{\partial \tau}dt \\ * * * & * * * & * * * & \int_0^T\left(\frac{\partial v_b}{\partial \tau}\right)^2 dt \end{pmatrix} \tag{8}$$

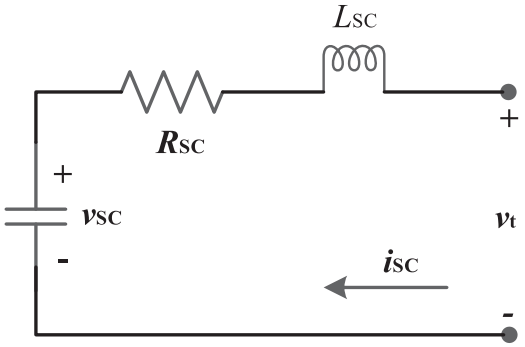

Fig. 4. ECM of an SC.

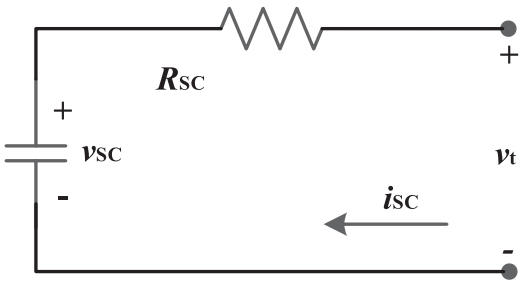

Fig. 5. Simplified SC ECM.

To obtain the ECM parameters of the SC module, its impedance spectra and crossover frequency f_c are measured when it is empty (i.e., the SC voltage is 0 V). f_c is about 80 Hz, thus the inductance L_{SC} can be calculated as follows:

$$L_{\mathrm{SC}} = \frac{1}{C_{\mathrm{SC}}(2\pi f_c)^2} \tag{13}$$

where C_{SC} is the capacitance of the SC module. For the adopted SC module, L_{SC} equals to 62.8 nH, which is very small and is, therefore, neglected. The goal of this paper is to estimate the HESS maximum power, thus the ECM for SC is simplified to an RC circuit, as shown in Fig. 5.

The dynamics of the SC ECM shown in Fig. 5 can be presented as

$$\begin{cases} v_t = v_{\mathrm{SC}} - R_{\mathrm{SC}} i_{\mathrm{SC}} \\ C_{\mathrm{SC}} \dot{v}_{\mathrm{SC}} = -i_{\mathrm{SC}} \end{cases} \tag{14}$$

where v_{SC} is the SC OCV, v_t is the SC terminal voltage, and i_{SC} is the SC current (positive for discharge and negative for charge). The derivative of v_t is given by

$$\dot{v}_t = -R_{\mathrm{SC}} \dot{i}_{\mathrm{SC}} - \frac{i_{\mathrm{SC}}}{C_{\mathrm{SC}}}. \tag{15}$$

Based on (15), the parametric model can be obtained as follows:

$$\dot{v}_t = {\theta_{\mathbf{SC}}}^T \mathbf{x_{SC}} \tag{16}$$

where

$$\begin{cases} \theta_{\mathbf{SC}} = \left[\frac{1}{C_{\mathrm{SC}}} \quad R_{\mathrm{SC}} \right]^T \\ \mathbf{x_{SC}} = \left[-i_{\mathrm{SC}} \quad -\dot{i}_{\mathrm{SC}} \right]^{\mathrm{T}}. \end{cases} \tag{17}$$

To obtain the CR bounds of the target parameters, the sinusoidal current shown in (18) is adopted as

$$i_{\mathrm{SC}}(t) = M \cos(\omega t). \tag{18}$$

Following the same procedures illustrated in Section II-A, the time-averaged Fisher matrix over a full cycle of sinusoidal current can be derived as

$$\bar{\mathbf{F}}_{\mathrm{SC}} = \begin{pmatrix} \frac{M^2}{2\sigma_V^2 \omega^2 C_{\mathrm{SC}}^4} & 0 \\ 0 & \frac{M^2}{2\sigma_V^2} \end{pmatrix}. \tag{19}$$

By inverting $\bar{\mathbf{F}}_{\mathrm{SC}}$, the CR bounds of C_{SC} and R_{SC} can be obtained as

$$\begin{cases} \underline{\sigma}(C_{\mathrm{SC}}) = \frac{\sqrt{2}\sigma_V \omega C_{\mathrm{SC}}^2}{M} \\ \underline{\sigma}(R_{\mathrm{SC}}) = \frac{\sqrt{2}\sigma_V}{M}. \end{cases} \tag{20}$$

It can be seen that the CR bounds of C_{SC} and R_{SC} do not have opposite requirements on the current frequency because $\underline{\sigma}(R_{\mathrm{SC}})$ is not influenced by ω. A distinct rule for improving the identification accuracy of both parameters is increasing the current amplitude *M* and reducing the noise in the measurement of v_t. The CR bound of C_{SC} monotonically increases with current frequency. Thus, a current excitation with large amplitude and low frequency is preferred.

III. Maximum Power Estimation

The maximum power of an HESS can be calculated based on its ECMs. Thus, the identified parameters illustrated in Section II are the basis to accurately estimate the HESS maximum power, which is one of most important decision factors in the EMS. Unlike battery-only and SC-only systems, the HESS is an over-actuated system. Optimal current components can, therefore, be integrated to simultaneously achieve accurate parameter identification and the desired output power. The HESS continuous maximum power over different prediction horizons is required for different applications. To be specific, the typical control period of EMS in vehicle applications is 1 s [2], thus the maximum power over 1 s should be estimated. Model predictive controller (MPC) can be a good choice for an HESS EMS [37], so the maximum power over the MPC prediction horizon, which generally consists of several control periods (e.g., 30 s), needs to be estimated. In grid applications, the EMS optimizes the energy storage system hourly [38], therefore, the maximum power over hours is essential for EMS to make a decision. Specifically, the maximum power information of HESS with different prediction horizons provides energy storage owners with valuable guidelines to better schedule and procure future services. Therefore, the HESS can be better utilized, which can potentially increase the benefit in grid applications.

In this paper, the maximum continuous power of battery and SC, which represent their capabilities of continuously supplying power to loads over the prediction horizon, are estimated simultaneously, and then the maximum total power of the HESS can be obtained by combining the above estimates. The maximum continuous currents of battery and SC over the prediction horizon are required in the estimation process of the

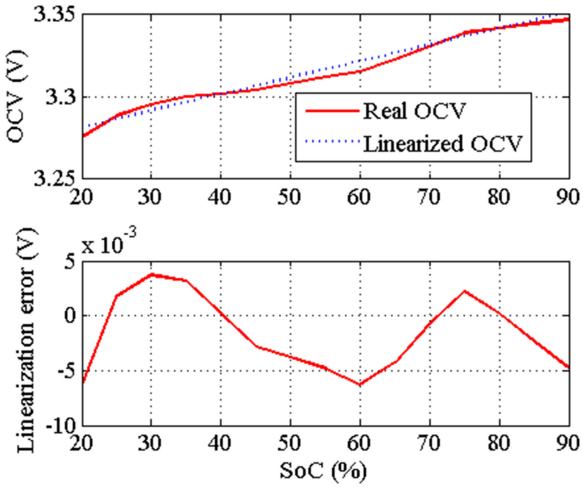

Fig. 6. OCV-SoC curve of the adopted battery cell.

maximum continuous power. The maximum continuous power of the HESS over 1 and 30 s is investigated in this section.

A. Maximum Power of Battery Pack

Based on (1), the battery model in discrete form can be given as

$$\begin{cases} v_C\left(k+1\right) = e^{-\frac{\Delta t}{\tau}} v_C\left(k\right) + i_b\left(k+1\right) R_t\left(1-e^{-\frac{\Delta t}{\tau}}\right) \\ v_b\left(k+1\right) = V_{\mathrm{OC}}\left(z_{k+1}\right) - v_C\left(k+1\right) - i_b\left(k+1\right) R_s \end{cases} \tag{21}$$

where k is the time step and Δt is the time interval between two consecutive steps. The battery SoC is denoted as z, which is the ratio of the remaining capacity to the available capacity [39]

$$z_{k+1} = z_k - \frac{i_{\mathrm{b}}\left(k+1\right)\Delta t}{Q_{\mathrm{bat}}} \tag{22}$$

where Q_{bat} is the battery capacity. As shown in (22), the battery OCV is a function of SoC. Thus, the maximum current under voltage limitation cannot be solved directly from (21). The battery OCV is typically a nonlinear function of SoC, as shown in Fig. 6. In order to simplify the solution, a local linearization of the OCV-SoC relationship is employed [27]

$$V_{\mathrm{OC}}\left(z_{k+1}\right) = V_{\mathrm{OC}}\left(z_k\right) - \frac{i_b\left(k+1\right)\Delta t}{Q_{\mathrm{bat}}} \frac{dV_{\mathrm{OC}}\left(z\right)}{dz}\bigg|_{z=z_k}. \tag{23}$$

As shown in Fig. 6, although the OCV-SoC can be linearized during the whole SoC usage window (20% to 90% with linearization error less than 5 mV) for the used battery, the general approach for simplifying the OCV-SoC relationship is local linearization. Thus, the SoC variation should be small when (23) is adopted. In addition, battery parameters including R_s, R_t, and τ, which are used in (21), are also influenced by the battery SoC. This means that the prediction horizon cannot be very long in order to ensure the estimation accuracy. In this paper, the prediction horizon is less than 30 s, over which there will not be significant SoC variations.

For safe operation, the SoC, voltage, and current of the battery must be restricted within a range [40], and the battery power will be limited by these restrictions. The maximum continuous current of the battery is 300 A. The maximum discharge/charge currents (i.e., the continuous maximum current over period Δt) under voltage limitations $I^{\mathrm{bat},V}_{\mathrm{dis,max}}/I^{\mathrm{bat},V}_{\mathrm{ch,max}}$ can be calculated by substituting $v_b(k+1)$ with the minimum/maximum battery voltages $V_{\mathrm{bat,min}}/V_{\mathrm{bat,max}}$ in (21) and (23), which is given as

$$\begin{cases} i^{\mathrm{bat},V}_{\mathrm{dis,max}} = \dfrac{V_{\mathrm{OC}}\left(z_k\right) - e^{-\frac{\Delta t}{\tau}} V_C\left(k\right) - V_{\mathrm{bat,min}}}{\frac{\Delta t}{Q_{\mathrm{bat}}} \frac{dV_{\mathrm{OC}}\left(z\right)}{dz}\Big|_{z=z_k} + R_t\left(1-e^{-\frac{\Delta t}{\tau}}\right) + R_s} \\ i^{\mathrm{bat},V}_{\mathrm{ch,max}} = \dfrac{V_{\mathrm{OC}}\left(z_k\right) - e^{-\frac{\Delta t}{\tau}} V_C\left(k\right) - V_{\mathrm{bat,max}}}{\frac{\Delta t}{Q_{\mathrm{bat}}} \frac{dV_{\mathrm{OC}}\left(z\right)}{dz}\Big|_{z=z_k} + R_t\left(1-e^{-\frac{\Delta t}{\tau}}\right) + R_s}. \end{cases} \tag{24}$$

When the battery SoC is close to its upper limit $z_{\max}$, the maximum charging current may also be limited by the SoC. Similarly, the maximum discharging current may be limited by SoC when the battery SoC is close to its lower limit $z_{\min}$. The maximum current estimation under SoC limitation can be given as

$$\begin{cases} i^{\mathrm{bat,SoC}}_{\mathrm{dis,max}} = \dfrac{\left(z_k - z_{\min}\right) Q_{\mathrm{bat}}}{\Delta t} \\ i^{\mathrm{bat,SoC}}_{\mathrm{ch,max}} = \dfrac{\left(z_k - z_{\max}\right) Q_{\mathrm{bat}}}{\Delta t}. \end{cases} \tag{25}$$

The battery is connected with the dc bus via a dc/dc converter, so the maximum current of the dc/dc converter inductor $i_{L,\max}$ should be considered. Based on the above analysis, the maximum current for prediction horizon Δt can be derived as

$$\begin{cases} i^{\mathrm{bat}}_{\mathrm{dis,max}} = \min\left(i^{\mathrm{bat},I}_{\mathrm{dis,max}},\ i^{\mathrm{bat},V}_{\mathrm{dis,max}},\ i^{\mathrm{bat,SoC}}_{\mathrm{dis,max}},\ i_{L,\max}\right) \\ i^{\mathrm{bat}}_{\mathrm{ch,max}} = \max\left(i^{\mathrm{bat},I}_{\mathrm{ch,max}},\ i^{\mathrm{bat},V}_{\mathrm{ch,max}},\ i^{\mathrm{bat,SoC}}_{\mathrm{ch,max}},\ -i_{L,\max}\right). \end{cases} \tag{26}$$

Finally, the discharge/charge maximum power of the battery $P^{\mathrm{bat}}_{\mathrm{dis,max}}/P^{\mathrm{bat}}_{\mathrm{ch,max}}$ can be obtained based on (26) and (27). Equation (27) is shown at the bottom of next page.

The maximum power of the battery pack for 1 s (i.e., Δt) can be estimated according to the above procedures. This is enough for most existing EMS, as a typical control update period of EMS is also 1 s [41]. However, for some specific EMS (e.g., the model predictive control strategy), the prediction horizon should be multiple control update periods [42]. Assuming the prediction horizon T is $N{\cdot}\Delta t$ (N is a positive integer, no more than 30 in this paper), the maximum power of the battery pack can be obtained by replacing Δt with $N{\cdot}\Delta t$ in (24), (25), and (27), as the maximum power estimation is based on a linearized model.

B. Maximum Power of SC Pack

The SC SoC is proportional to its voltage, thus only the voltage and current constraints need to be considered to estimate its maximum power. Based on (14), the discrete time SC model can be derived as

$$\begin{cases} v_{\mathrm{SC}}\left(k+1\right) = v_{\mathrm{SC}}\left(k\right) - \frac{i_{\mathrm{SC}}(k+1)}{C_{\mathrm{SC}}}\Delta t \\ v_t\left(k+1\right) = v_{\mathrm{SC}}\left(k+1\right) - i_{\mathrm{SC}}\left(k+1\right) R_{\mathrm{SC}}. \end{cases} \tag{28}$$

The maximum SC voltage $V_{\mathrm{SC,max}}$ is the voltage when the SC is fully charged. Generally, the SC terminal voltage is strictly controlled between $0.5\mathrm{V}_{\mathrm{SC,max}}$ and $V_{\mathrm{SC,max}}$ as the efficiency of power conversion becomes poor when v_{SC} is low. Unlike the battery, the SC voltage changes relatively quickly when the current is large. If the SC power is constant over a prediction horizon, the SC discharge current will increase and the SC charge current decreases due to the change in voltage, especially when the prediction horizon is long. Thus, the maximum power of SC cannot be calculated in the same way as the battery. The SC maximum power is definitely limited by its voltage. In addition, the maximum power is also limited by the continuous maximum currents allowed by the inductor and manufacturer. The maximum continuous current of the SC module is 240 A at 40 °C, therefore, the maximum discharge/charge current $i^{\mathrm{SC}}_{\mathrm{dis,con}}/i^{\mathrm{SC}}_{\mathrm{ch,con}}$ is set to 240 A/–240 A. The maximum power under both the voltage and current limitations can be given as

$$P^{\mathrm{SC},IV}_{\mathrm{dis,max}} = \begin{cases} \frac{1}{2}C_{\mathrm{SC}}\dfrac{\left(v^2_{\mathrm{SC}}(k)-\left(v_{\mathrm{SC}}(k)-\frac{i^{\mathrm{SC}}_{\mathrm{dis,con}}\Delta t}{C_{\mathrm{SC}}}\right)^2\right)}{\Delta t} \\ \frac{i^{\mathrm{SC}}_{\mathrm{dis,con}}\Delta t}{C_{\mathrm{SC}}} \le v_{\mathrm{SC}}(k) - 0.5\mathrm{V}_{\mathrm{SC,max}} \\ \frac{1}{2}C_{\mathrm{SC}}\dfrac{\left(v^2_{\mathrm{SC}}(k)-0.25\mathrm{V}^2_{\mathrm{SC,max}}\right)}{\Delta t} \\ \frac{i^{\mathrm{SC}}_{\mathrm{dis,con}}\Delta t}{C_{\mathrm{SC}}} > v_{\mathrm{SC}}(k) - 0.5\mathrm{V}_{\mathrm{SC,max}} \end{cases} \tag{29}$$

$$P^{\mathrm{SC},IV}_{\mathrm{ch,max}} = \begin{cases} \frac{1}{2}C_{\mathrm{SC}}\dfrac{\left(v^2_{\mathrm{SC}}(k)-\left(v_{\mathrm{SC}}(k)-\frac{i^{\mathrm{SC}}_{\mathrm{ch,con}}\Delta t}{C_{\mathrm{SC}}}\right)^2\right)}{\Delta t} \\ \frac{i^{\mathrm{SC}}_{\mathrm{ch,con}}\Delta t}{C_{\mathrm{SC}}} \ge v_{\mathrm{SC}}(k) - V_{\mathrm{SC,max}} \\ \frac{1}{2}C_{\mathrm{SC}}\dfrac{\left(v^2_{\mathrm{SC}}(k)-V^2_{\mathrm{SC,max}}\right)}{\Delta t} \\ \frac{i^{\mathrm{SC}}_{\mathrm{ch,con}}\Delta t}{C_{\mathrm{SC}}} < v_{\mathrm{SC}}(k) - V_{\mathrm{SC,max}}. \end{cases} \tag{30}$$

Finally, the discharge/charge maximum power of SC, $P^{\mathrm{SC}}_{\mathrm{dis,max}}/P^{\mathrm{SC}}_{\mathrm{ch,max}}$, can be obtained considering the resistance

$$\begin{cases} P^{\mathrm{SC}}_{\mathrm{dis,max}} = P^{\mathrm{SC},IV}_{\mathrm{dis,max}} - \left(\dfrac{P^{\mathrm{SC},IV}_{\mathrm{dis,max}}}{\sqrt{v^2_{\mathrm{SC}}(k)-2P^{\mathrm{SC},IV}_{\mathrm{dis,max}}\Delta t/C_{\mathrm{SC}}}}\right)^2 R_{\mathrm{SC}} \\ P^{\mathrm{SC}}_{\mathrm{ch,max}} = P^{\mathrm{SC},IV}_{\mathrm{ch,max}} + \left(\dfrac{P^{\mathrm{SC},IV}_{\mathrm{ch,max}}}{v_{\mathrm{SC}}(k)}\right)^2 R_{\mathrm{SC}}. \end{cases} \tag{31}$$

Similarly, the maximum power of the SC pack for N time intervals can be obtained by replacing Δt with $N{\cdot}\Delta t$ in (29)–(31). Based on above analysis, the maximum power of HESS can be obtained as follows: where $P^{\mathrm{HESS}}_{\mathrm{dis,max}}$ and $P^{\mathrm{HESS}}_{\mathrm{ch,max}}$ are the maximum discharging and charging power of the HESS, and $R_{D,\mathrm{bat}}$ and $R_{D,\mathrm{SC}}$ are the dc/dc converter resistances associated with the battery and SC, respectively. In the test-bed, the inductors for both battery and SC packs are designed to have a maximum current of 300 A, which satisfies the maximum currents requirement of both battery and SC.

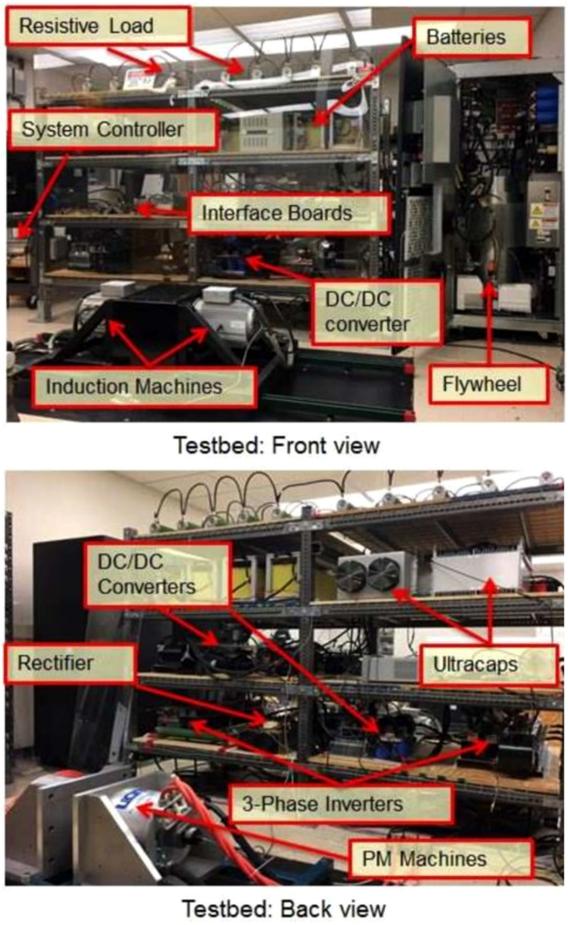

Fig. 7. HESS test-bed.

As shown in (27) and (32) shown at the bottom of the next page, the maximum continuous power calculation processes of battery and SC require accurate parameters of the corresponding ECMs. So, the parameters should be accurately identified by adopting the optimal excitation currents, which can be designed based on the analysis results in Section II.

IV. Experimental Results and Discussions

An experimental test-bed has been constructed, as shown in Fig. 7. This test-bed provides a flexible platform for the experimental validation of HESS. The dc/dc converters, which are controlled by a central microprocessor, distribute the power request between the battery and SC as well as generate exciting signals for parameter identification. To simulate the fully active HESS adopted in this paper, both the battery and SC packs of the test-bed are connected to the dc bus via dc/dc converters. The resistive load consists of 19 100-Ω resistors connected

$$\begin{cases} P^{\mathrm{bat}}_{\mathrm{dis,max}} = \left[V_{\mathrm{OC}}(z_{k+1}) - e^{-\frac{\Delta t}{\tau}}v_C(k) - i^{\mathrm{bat}}_{\mathrm{dis,max}}R_t\left(1-e^{-\frac{\Delta t}{\tau}}\right) - i^{\mathrm{bat}}_{\mathrm{dis,max}}R_s\right] i^{\mathrm{bat}}_{\mathrm{dis,max}} \\ P^{\mathrm{bat}}_{\mathrm{ch,max}} = \left[V_{\mathrm{OC}}(z_{k+1}) - e^{-\frac{\Delta t}{\tau}}v_C(k) - i^{\mathrm{bat}}_{\mathrm{ch,max}}R_t\left(1-e^{-\frac{\Delta t}{\tau}}\right) - i^{\mathrm{bat}}_{\mathrm{ch,max}}R_s\right] i^{\mathrm{bat}}_{\mathrm{ch,max}} \end{cases} \tag{27}$$

TABLE I
SPECIFICATIONS FOR THE BATTERY PACK

LiFePO4 Battery	
Manufacturer	Flux Power® (BMS) & Winston® (cells)
Cell voltage limits (V)	2.5/3.9
Max. continuous current (A)	300
Capacity (Ah)	100
DC voltage (V)	36-144
Battery pack resistance (Ω)	0.08
Communication Interface	CAN bus

TABLE II
SPECIFICATIONS FOR THE SC MODULE

SC Module	
Manufacturer	Maxwell Technologies®
Rated Capacitance (F)	63
Rated Voltage (V)	125
Max. continuous current at 40°C (A)	240
Max. equivalent series resistance (mΩ)	18

in parallel. The load profile can be realized by controlling the duty cycle of another dc/dc converter that is used to connect the resistive load and dc bus. Detailed information about the test-bed construction is provided in [43]. When the power demand is constant, the excitation current can be directly applied to the battery and the excitation current for SC can be inherently generated because the dc-bus voltage is regulated to be constant by a Lyapunov-function-based controller, proposed in [8].

The battery pack in the test-bed consists of 48 LiFePO4 cells that are connected in series. A battery management system (BMS) from Flux Power utilizes a distributed architecture where every BMS module manages four cells via passive (i.e., resistive shunting) cell balancing. The battery current is measured by the BMS to estimate the SoC of the pack. The specifications of the battery pack are listed in Table I.

In the test-bed, two SC modules are connected in series within the SC pack. Manufacturer specifications for the SC module are provided in Table II.

The analysis in Section II shows that appropriate excitation should be applied to both battery and SC to achieve high identification accuracy. For the battery-only configuration, the current profile of the battery is directly determined by the power demand, therefore, it is practically impossible to design the current profile. However, HESS including both battery and SC is an overactuated system, which provides an opportunity to achieve sufficiently rich input signals and output regulation objectives simultaneously. Although the power demand is constant in this paper, we point out that the HESS has the capability of providing rich input signals for parameter identification processes when the power demand varies with time. In addition, we point out that the sinusoidal current need not be injected all the time, as the battery and SC parameters do not change quickly. The specific remark can be given as follows.

Remark #1: The implications of injecting a current signal for active parameter estimation could be problematic for general applications. In this paper, however, we focus on the battery/SC HESS, which is an overactuated system and provides an opportunity to achieve sufficiently rich input signals and output regulation objectives simultaneously. Therefore, the optimal current signal can be directly injected, and the negative influence of injecting the 10 A current in the experiment on the HESS performance (i.e., system efficiency and power supply quality) can be minimized given the HESS overactuated nature. Specifically, for any power demand P_d, we have $P_d = P_{s1} + P_{s2}$, where P_{s1} and P_{s2} are the power from source 1 (i.e., battery) and source 2 (i.e., SC).

The analysis in Section II shows that both battery and SC demand a low-frequency current component in the parameter identification process. As shown in Fig. 3, when $k = 2$, sinusoids with frequencies of 0.004 and 0.008 Hz are optimal to achieve satisfactory performance in the combined identification process of the battery packs. This low optimal frequency, however, imposes several problems, as it requires a long identification period. Thus, in our experiment, sinusoids with frequencies of 0.02 and 0.04 Hz (the amplitudes of both waveforms are $M = 5$ A), which also have slow component, are used for the battery pack. Based on the voltage controller, the SC current profile is generated as shown in Fig. 8.

An RLS with a constant forgetting factor of 0.992 is used to identify the parameters of the battery pack, and the battery SoC is maintained at around 55% during the experiment. The derivative of the battery and SC voltages are adopted in this paper to avoid more states in the identification process. However, the derivative of voltage can be pretty noisy in real applications, which will, therefore, impair the estimation performance. An averaging filter can be used to solve this problem. For the parameter identification with optimal current profiles (i.e., the frequencies of the battery current are 0.004 and 0.008 Hz), the window length of the average filters for both battery and SC contains ten samples. Since the sampling frequency is 2 Hz, the averaging filter, which has a low-pass function, has a –10 dB

$$\begin{cases} P^{\mathrm{HESS}}_{\mathrm{dis,max}} = P^{\mathrm{bat}}_{\mathrm{dis,max}} + P^{\mathrm{SC}}_{\mathrm{dis,max}} - \left[\left(i^{\mathrm{bat}}_{\mathrm{ch,max}} \right)^2 R_{\mathrm{D,bat}} + \left(\frac{P^{\mathrm{SC},IV}_{\mathrm{dis,max}}}{\sqrt{v^2_{\mathrm{SC}}(k) - 2P^{\mathrm{SC},IV}_{\mathrm{dis,max}} \Delta t / C_{\mathrm{SC}}}} \right)^2 R_{\mathrm{D,SC}} \right] \\ P^{\mathrm{HESS}}_{\mathrm{ch,max}} = P^{\mathrm{bat}}_{\mathrm{ch,max}} + P^{\mathrm{SC}}_{\mathrm{ch,max}} + \left[\left(i^{\mathrm{bat}}_{\mathrm{ch,max}} \right)^2 R_{\mathrm{D,bat}} + \left(\frac{P^{\mathrm{SC},IV}_{\mathrm{ch,max}}}{v_{\mathrm{SC}}(k)} \right)^2 R_{\mathrm{D,SC}} \right] \end{cases} \tag{32}$$

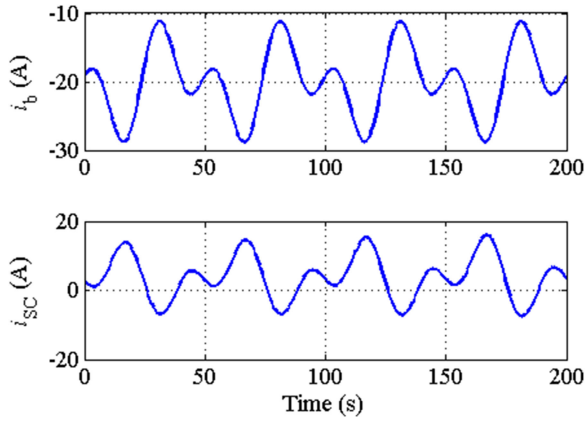

Fig. 8. Excitation current profiles for battery and SC.

bandwidth of 0.105 Hz. We point out that the averaging filter should be designed considering the sampling frequency. When the sampling frequency increases, the window length of the average filter should also increase to achieve the same bandwidth. Based on (2), the filtered system in continuous-time can be given as

$$v_b(s)\frac{T_c}{s+T_c} = \frac{1}{s}V_{\mathrm{OC}}\frac{T_c}{s+T_c} - R_s i_b(s)\frac{T_c}{s+T_c} - \frac{R_t}{1+\tau s}i_b(s)\frac{T_c}{s+T_c} \tag{33}$$

where T_c is the time coefficient of the low-pass filter. Since V_{OC} is considered as a constant in the identification process, the filtered system is provided as

$$v_{\mathrm{bf}}(s) = \frac{1}{s}V_{\mathrm{OC}} - R_s i_{\mathrm{bf}}(s) - \frac{R_t}{1+\tau s}i_{\mathrm{bf}}(s) \tag{34}$$

where v_{bf} and i_{bf} are the filtered voltage and current, respectively. The parameters can then be identified based on the filtered dynamics.

As shown in Fig. 9, the ohmic resistance R_s is about 60 mΩ and R_t is about 187 mΩ. The battery pack time constant τ is about 60 s. Based on the identification result, the terminal voltage can be estimated accordingly.

As shown in Fig. 10, the estimated terminal voltage can accurately track the real one as estimation error is below 0.5%, which means that the first-order ECM can accurately represent the battery dynamic. All parameters shown in Fig. 9 are vital to the maximum power estimation of the battery. The optimal current profile is necessary for parameter identification, and accurate parameters can achieve accurate maximum power estimation. The sampling period of the identification process is 0.5 s, and the computer (with Intel(R) Core(TM) i7 Cpu/16G RAM) takes 0.023291 s for the 200 s identification process, which is satisfactory. But we point out that the sampling time can be slightly increased to 2 s, while the identification performance can also be guaranteed with a computation time of 0.010948 s. When the identification problem becomes more complex, it is worth increasing the sampling time in practical applications.

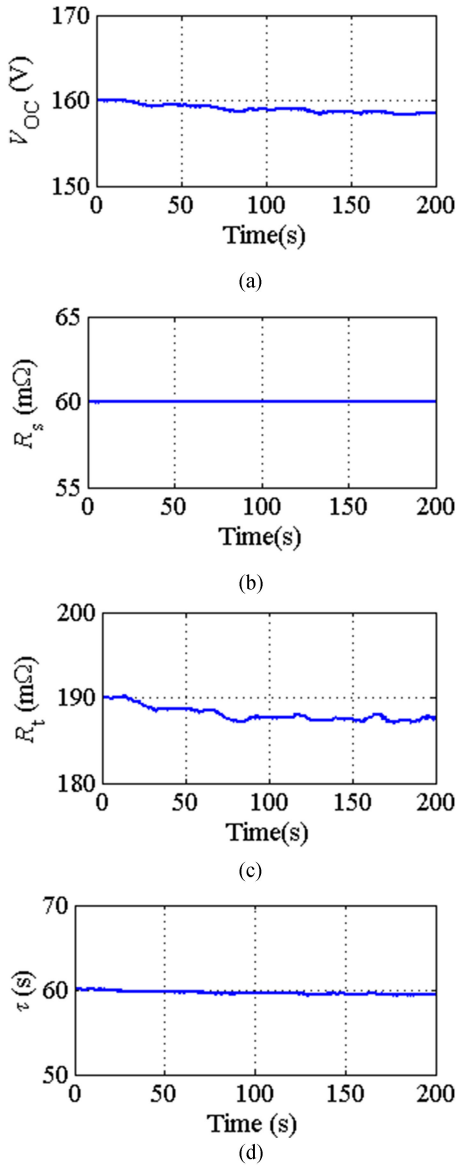

Fig. 9. Parameter identification results of battery pack. (a) V_{OC}. (b) R_s. (c) R_t. (d) τ.

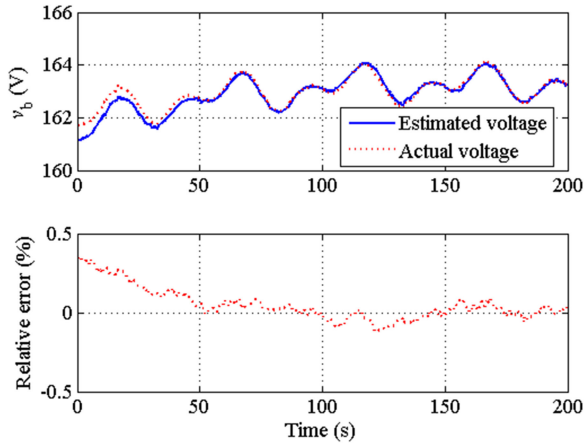

Fig. 10. Terminal voltage estimation result of the battery pack.

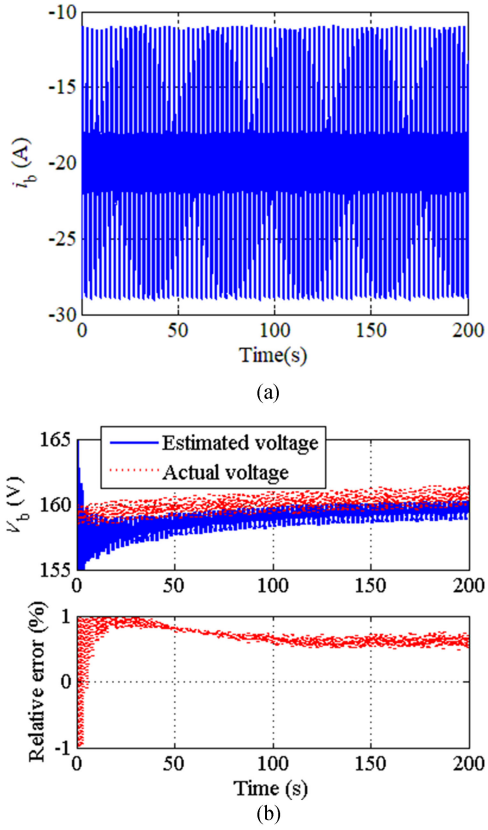

Fig. 11. Parameter identification results under the nonoptimal current profile. (a) Current profile. (b) Terminal voltage estimation result.

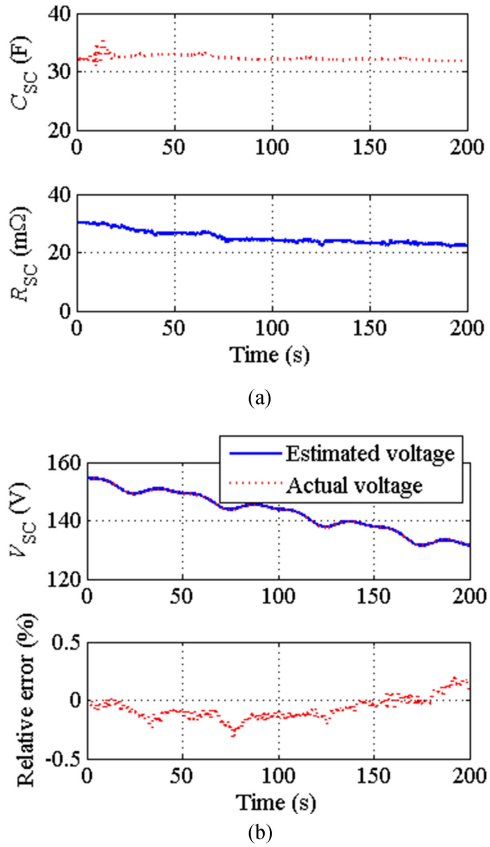

Fig. 12. Parameter identification results of the SC pack. (a) Parameter identification results. (b) Terminal voltage estimation result.

To further verify the accuracy of the provided analysis, the frequencies of the sine waves were increased to 0.4 and 0.8 Hz, which are twenty times higher than the ones in the original experiment. The sampling period of the identification process is 0.01 s. As shown in Fig. 11(b), the estimation error of the terminal voltage increases significantly and is more than 0.5%. Based on the comparison results, the conclusion can be, therefore, drawn that the nonoptimal frequencies of the sine waves shown in Fig. 11(a) lead to larger error variance.

The RLS with a constant forgetting factor of 0.996 was then used to identify the parameters of the SC pack. We point out that it is difficult to automatically determine the optimal forgetting factor. The selected forgetting factors (i.e., 0.992 for battery and 0.996 for SC) are based on tuning results, which found that the selected ones achieved the best estimation performance. Generally, a small forgetting factor is used in the case that the estimated parameters change quickly via time, therefore, the previous data, which contains the parameter information in the past, is no longer relevant. For the battery and the SC studied in this paper, the parameters do not quickly change, so a larger forgetting factor is preferred.

The sampling period of the SC parameter identification was set to 0.5 s. As shown in Fig. 12(a), the SC capacity C_{SC} is about 31.5 F (the nominal capacity of the SC pack is also 31.5 F) and its ohmic resistance R_s is about 20 mΩ. As shown in Fig. 12(b), the estimated terminal voltage of the SC pack can accurately track the actual value with an error below 0.5%. Thus, the simplified ECM can accurately represent the SC dynamic, and it can be used to estimate the SC maximum power.

The above experimental results show that the ECMs used in this paper can simulate the system dynamics accurately using the optimal excitation current profiles. Based on the appropriate ECMs and the accurate identified parameters, the maximum power of HESS can be then estimated. Maximum discharge/charge currents of the battery are shown in Fig. 13(a). Maximum currents under SoC limitation are much larger and not given because the battery SoC is not near its upper and lower bounds (i.e., 55% in the experiment). It can be seen that, when the prediction horizon is longer (i.e., 30 s), maximum currents decrease for the battery due to the voltage limitation [40], and thus, may become the main factor influencing the maximum power of the battery. For a short prediction horizon (i.e., 1 s), maximum currents under voltage limitation are larger than the ones under manufacturer limitation. This result may change when the battery SoC is very close to its limitations. In the experiment, both the battery discharge and charge currents for 1 s are restricted by the saturation current of the dc/dc converter inductor.

The HESS maximum power for the next sampling interval, which is generally 1 s, is particularly important to restrict the HESS power in practical applications [2]. In some specific cases, for example, the MPC requires a long estimation horizon, and an accurate HESS maximum power is really critical in the

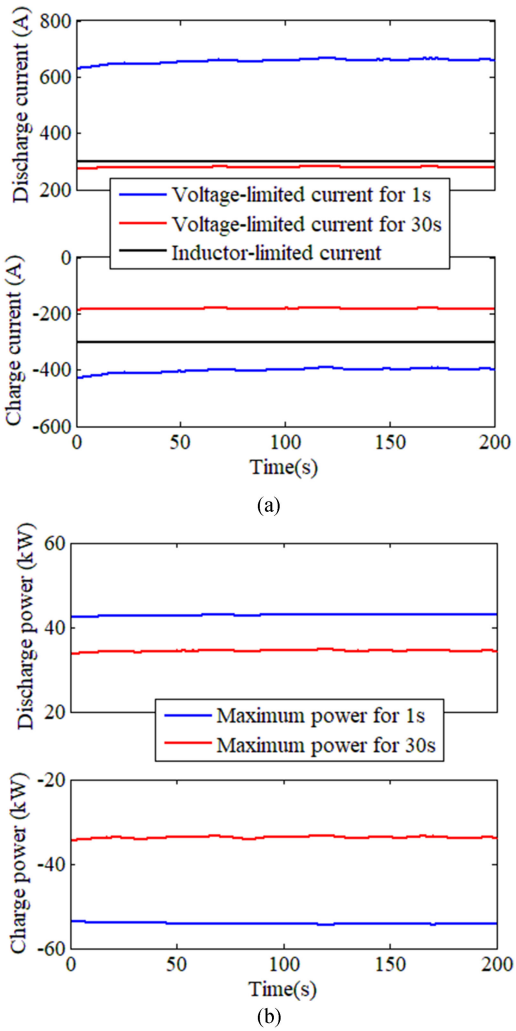

Fig. 13. Maximum power estimation results of the battery pack. (a) Current limitations. (b) Maximum power under discharge/charge processes.

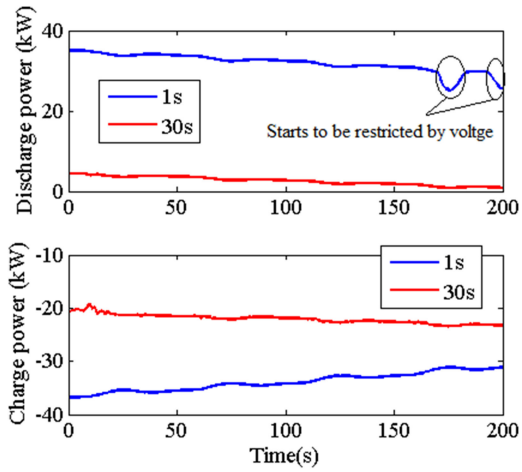

Fig. 14. Maximum power estimation results of SC pack.

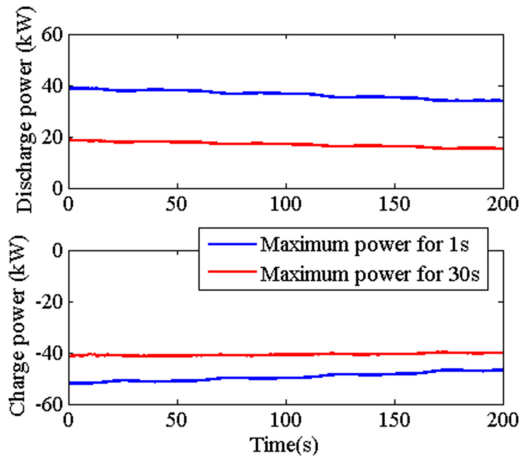

Fig. 15. Maximum power estimation result of HESS.

algorithm [42]. Therefore, in this paper, the results for different prediction horizons are investigated. The battery maximum power can be calculated according to (26) and (27), and the battery maximum power for 30 s is smaller than the one for 1 s, as shown in Fig. 13(b).

The estimation result for the SC pack is shown in Fig. 14. The maximum discharge power for 1 s is much larger than the one for 30 s. Maximum continuous discharge/charge powers for 30 s are strictly limited by SC voltage. In terms of the large prediction horizon, the SC voltage is likely to restrict the maximum power. When the prediction horizon decreases, the SC maximum current tends to limit its maximum power. As shown in Fig. 14, the maximum charge power for 1 s, which is strictly restricted by the maximum current requirement, is large and does not contain any ripple because the SC voltage is relatively low in the experiment. It is difficult to reach the upper bound when the SC voltage is low, since its current is also limited. For the maximum discharge power for 1 s, it is initially restricted by the current limitation, but at the last stage, the SC voltage begins to limit its maximum power as the SC voltage is approaching its lower bound. Besides the maximum current and voltage limitations, the maximum power also depends on the time period for draining the available energy. As a result, the maximum power decreases as the prediction horizon increases.

Based on (32), power loss caused by the inductor resistance can be estimated and the HESS maximum power can be obtained, as shown in Fig. 15. Generally, the maximum power for short duration is significantly larger than for longer duration. The maximum power estimation can be adopted in the HESS EMS for online uses (e.g., vehicle [4] and grid [44] applications).

V. Conclusion

This paper presents the analysis, design, and experimental validation of parameter identification of a battery/SC HESS for system monitoring and maximum power estimation. Based on the Fisher information matrix and CR bound analysis, the parameter identification accuracy is analyzed considering noise in measurements. It is shown that appropriate current profiles should be adopted to properly excite both battery and SC. Therefore, identification accuracy can be guaranteed.

An HESS including both battery and SC is an overactuated system, which provides an opportunity to achieve sufficiently rich input signals and output regulation objectives simultaneously. The power demand is assumed to be constant in this paper to simplify the problem. However, we point out that the optimal current signal can be directly injected when the power demand is varying, and the negative influence of injecting the excitation current on the HESS performance (i.e., system efficiency and power supply quality) can be minimized given the HESS overactuated nature. Both the battery and SC need low frequency current components to achieve a satisfactory identification performance. Based on these excitation current profiles, the parameters of battery and SC are identified using RLS with a forgetting factor. The experimental results show that the accuracy of the simplified ECM is satisfactory when the current profile is well designed. Based on the identified parameters, the maximum power of the battery and SC are estimated for different time horizons (i.e., 1 and 30 s). The maximum power for short durations is significantly larger than the one for long durations. We point out that the analysis and parameter identification algorithm can be generalized to the systems including either battery or SC.

In future work, the parameter identification and system optimization will be considered together in the EMS to optimize the comprehensive performance.

REFERENCES

[1] L. Xue, Z. Shen, D. Boroyevich, P. Mattavelli, and D. Diaz, "Dual active bridge-based battery charger for plug-in hybrid electric vehicle with charging current containing low frequency ripple," *IEEE Trans. Power Electron.*, vol. 30, no. 12, pp. 7299–7307, Dec. 2015.

[2] Z. Song *et al.*, "Multi-objective optimization of a semi-active battery/supercapacitor energy storage system for electric vehicles," *Appl. Energy*, vol. 135, pp. 212–224, 2014.

[3] O. Laldin, M. Moshirvaziri, and O. Trescases, "Predictive algorithm for optimizing power flow in hybrid ultracapacitor/battery storage systems for light electric vehicles," *IEEE Trans. Power Electron.*, vol. 28, no. 8, pp. 3882–3895, Aug. 2013.

[4] Z. Song, H. Hofmann, J. Li, X. Han, X. Zhang, and M. Ouyang, "A comparison study of different semi-active hybrid energy storage system topologies for electric vehicles," *J. Power Sources*, vol. 274, pp. 400–411, 2015.

[5] R. A. Dougal, S. Liu, and R. E. White, "Power and life extension of battery-ultracapacitor hybrids," *IEEE Trans. Compon. Packag. Technol.*, vol. 25, no. 1, pp. 120–131, Mar. 2002.

[6] D. B. W. Abeywardana, B. Hredzak, and V. G. Agelidis, "Single-phase grid-connected $LiFePO_4$ battery–supercapacitor hybrid energy storage system with interleaved boost inverter," *IEEE Trans. Power Electron.*, vol. 30, no. 10, pp. 5591–5604, Oct. 2015.

[7] B. Hredzak, V. G. Agelidis, and M. Jang, "A model predictive control system for a hybrid battery-ultracapacitor power source," *IEEE Trans. Power Electron.*, vol. 29, no. 3, pp. 1469–1479, Mar. 2014.

[8] Z. Song, J. Hou, H. Hofmann, J. Li, and M. Ouyang, "Sliding-mode and Lyapunov function-based control for battery/supercapacitor hybrid energy storage system used in electric vehicles," *Energy*, vol. 122, pp. 601–612, 2017.

[9] Y. Zhang, R. Xiong, H. He, and W. Shen, "Lithium-ion battery pack state of charge and state of energy estimation algorithms using a hardware-in-the-loop validation," *IEEE Trans. Power Electron.*, vol. 32, no. 6, pp. 4421–4431, Jun. 2017.

[10] Q. K. Wang, Y. J. He, J. N. Shen, X. Hu, and Z. F. Ma, "State of charge-dependent polynomial equivalent circuit modeling for electrochemical impedance spectroscopy of lithium-ion batteries," *IEEE Trans. Power Electron.*, vol. 33, no. 10, pp. 8449–8460, Oct. 2017.

[11] H. Aung, K. S. Low, and S. T. Goh, "State-of-charge estimation of lithium-ion battery using square root spherical unscented Kalman filter (Sqrt-UKFST) in nanosatellite," *IEEE Trans. Power Electron.*, vol. 30, no. 9, pp. 4774–4783, Sep. 2015.

[12] H. Gualous, D. Bouquain, A. Berthon, and J. M. Kauffmann, "Experimental study of supercapacitor serial resistance and capacitance variations with temperature," *J. Power Sources*, vol. 123, no. 1, pp. 86–93, 2003.

[13] J. Poon, P. Jain, C. Spanos, S. K. Panda, and S. R. Sanders, "Fault prognosis for power electronics systems using adaptive parameter identification," *IEEE Trans.Ind. Appl.*, vol. 53, no. 3, pp. 2862–2870, May/Jun. 2017.

[14] X. Hu, S. Li, and H. Peng, "A comparative study of equivalent circuit models for Li-ion batteries," *J. Power Sources*, vol. 198, pp. 359–367, 2012.

[15] A. Eddahech, M. Ayadi, O. Briat, and J. M. Vinassa, "Online parameter identification for real-time supercapacitor performance estimation in automotive applications," *Int. J. Elect. Power Energy Syst.*, vol. 51, pp. 162–167, 2013.

[16] J. Meng, G. Luo, and F. Gao, "Lithium polymer battery state-of-charge estimation based on adaptive unscented Kalman filter and support vector machine," *IEEE Trans. Power Electron.*, vol. 31, no. 3, pp. 2226–2238, Mar. 2016.

[17] H. Rahimi-Eichi, F. Baronti, and M. Y. Chow, "Online adaptive parameter identification and state-of-charge coestimation for lithium-polymer battery cells," *IEEE Trans. Ind. Electron.*, vol. 61, no. 4, pp. 2053–2061, Apr. 2014.

[18] X. Lin, A. G. Stefanopoulou, Y. Li, and R. D. Anderson, "State of charge imbalance estimation for battery strings under reduced voltage sensing," *IEEE Trans. Control Syst. Technol.*, vol. 23, no. 3, pp. 1052–1062, May 2015.

[19] X. Lin, and A. G. Stefanopoulou, "Analytic bound on accuracy of battery state and parameter estimation," *J. Electrochem. Soc.*, vol. 162, no. 9, pp. A1879–A1891, 2015.

[20] P. A. Ioannou, and J. Sun, *Robust Adaptive Control*, vol. 1. Upper Saddle River, NJ, USA: Prentice-Hall, 1996,

[21] X. Lin "Analytic analysis of the Data-Dependent estimation accuracy of battery equivalent circuit dynamics," *IEEE Control Syst. Lett.*, vol. 1, no. 2, pp. 304–309, Oct. 2017.

[22] M. J. Rothenberger, D. J. Docimo, M. Ghanaatpishe, and H. K. Fathy, "Genetic optimization and experimental validation of a test cycle that maximizes parameter identifiability for a Li-ion equivalent-circuit battery model," *J. Energy Storage*, vol. 4, pp. 156–166, 2015.

[23] A. Klintberg, T. Wik, and B. Fridholm, "Theoretical bounds on the accuracy of state and parameter estimation for batteries," in *Proc. Amer. Control Conf.*, May 2017, pp. 4035–4041.

[24] X. Lin "Theoretical analysis of battery SOC estimation errors under sensor Bias and variance," *IEEE Trans. Ind. Electron.*, vol. 65, no. 9, pp. 7138–7148, Sep. 2018.

[25] Y. Zheng, M. Ouyang, X. Han, L. Lu, and J. Li, "Investigating the error sources of the online state of charge estimation methods for lithium-ion batteries in electric vehicles," *J. Power Sources*, vol. 377, pp. 161–188, 2018.

[26] Z. Song, H. Hofmann, J. Li, X. Han, and M. Ouyang, "Optimization for a hybrid energy storage system in electric vehicles using dynamic programing approach," *Appl. Energy*, vol. 139, pp. 151–162, 2015.

[27] R. Xiong, H. He, F. Sun, X. Liu, and Z. Liu, "Model-based state of charge and peak power capability joint estimation of lithium-ion battery in plug-in hybrid electric vehicles," *J. Power Sources*, vol. 229, pp. 159–169, 2013.

[28] Z. Song, H. Hofmann, J. Li, J. Hou, X. Han, and M. Ouyang, "Energy management strategies comparison for electric vehicles with hybrid energy storage system," *Appl. Energy*, vol. 134, pp. 321–331, 2014.

[29] D. Montesinos-Miracle, M. Massot-Campos, J. Bergas-Jane, S. Galceran-Arellano, and A. Rufer, "Design and control of a modular multilevel DC/DC converter for regenerative applications," *IEEE Trans. Power Electron.*, vol. 28, no. 8, pp. 3970–3979, Aug. 2013.

[30] R. W. De Doncker, D. M. Divan, and M. H. Kheraluwala, "A three-phase soft-switched high-power-density DC/DC converter for high-power applications," *IEEE Trans. Ind. Appl.*, vol. 27, no. 1, pp. 63–73, Jan,/Feb. 1991.

[31] J. Gomez, R. Nelson, E. E. Kalu, M. H. Weatherspoon, and J. P. Zheng, "Equivalent circuit model parameters of a high-power Li-ion battery: Thermal and state of charge effects," *J. Power Sources*, vol. 196, no. 10, pp. 4826–4831, 2011.

[32] Y. H. Chiang, W. Y. Sean, and J. C. Ke, "Online estimation of internal resistance and open-circuit voltage of lithium-ion batteries in electric vehicles," *J. Power Sources*, vol. 196, no. 8, pp. 3921–3932, 2011.
[33] F. Sun, R. Xiong, and H. He, "Estimation of state-of-charge and state-of-power capability of lithium-ion battery considering varying health conditions," *J. Power Sources*, vol. 259, pp. 166–176, 2014.
[34] X. Hu, R. Xiong, and B. Egardt, "Model-based dynamic power assessment of lithium-ion batteries considering different operating conditions," *IEEE Trans. Ind. Inf.*, vol. 10, no. 3, pp. 1948–1959, Aug. 2014.
[35] A. Sharma, and H. K. Fathy, "Fisher identifiability analysis for a periodically-excited equivalent-circuit lithium-ion battery model," in *Proc. Amer. Control Conf.*, Jun. 2014, pp. 274–280.
[36] X. Hu, F. Sun, Y. Zou, and H. Peng, "Online estimation of an electric vehicle lithium-ion battery using recursive least squares with forgetting," in *Proc. Amer. Control Conf.*, Jun. 2011, pp. 935–940.
[37] J. Hou, J. Sun, and H. Hofmann, "Control development and performance evaluation for battery/flywheel hybrid energy storage solutions to mitigate load fluctuations in all-electric ship propulsion systems," *Appl. Energy*, vol. 212, pp. 919–930, 2018.
[38] C. T. Li, C. Ahn, H. Peng, and J. Sun, "Synergistic control of plug-in vehicle charging and wind power scheduling," *IEEE Trans. Power Syst.*, vol. 28, no. 2, pp. 1113–1121, May 2013.
[39] L. Lu, X. Han, J. Li, J. Hua, and M. Ouyang, "A review on the key issues for lithium-ion battery management in electric vehicles," *J. Power Sources*, vol. 226, pp. 272–288, 2013.
[40] T. Feng, L. Yang, X. Zhao, H. Zhang, and J. Qiang, "Online identification of lithium-ion battery parameters based on an improved equivalent-circuit model and its implementation on battery state-of-power prediction," *J. Power Sources*, vol. 281, pp. 192–203, 2015.
[41] Z. Song, H. Hofmann, J. Li, J. Hou, X. Zhang, and M. Ouyang, "The optimization of a hybrid energy storage system at subzero temperatures: Energy management strategy design and battery heating requirement analysis," *Appl. Energy*, vol. 159, pp. 576–588, 2015.
[42] J. Hou, J. Sun, and H. F. Hofmann, "Mitigating power fluctuations in electric ship propulsion with hybrid energy storage system: Design and analysis," *IEEE J. Ocean. Eng.*, vol. 43, no. 1, pp. 93–107, Jan. 2013.
[43] J. Hou, D. M. Reed, K. Zhou, H. Hofmann, and J. Sun, "Modeling and testbed development for an electric drive system with hybrid energy storage," in *Proc. Elect. Machines Technol. Symp.*, 2014.
[44] A. Aktas, K. Erhan, S. Ozdemir, and E. Ozdemir, "Experimental investigation of a new smart energy management algorithm for a hybrid energy storage system in smart grid applications," *Elect. Power Syst. Rese.*, vol. 144, pp. 185–196, 2017.

Ziyou Song (M'18) received the B.E. degree (with hons.) and the Ph.D. degree (with highest hons.) in automotive engineering from Tsinghua University, Beijing, China, in 2011 and 2016, respectively.

He is currently a Postdoctor with the University of Michigan, Ann Arbor, MI, USA. His research interests include battery parameter estimation, hybrid energy storage systems, and electric and hybrid electric vehicles.

Jun Hou (S'15) received the M.S. degrees in electrical engineering from Northeastern University, Shenyang, China, in 2011, and the Ph.D. degree from the University of Michigan, Ann Arbor, MI, USA, in 2017.

His current research interests include integration, modeling, control, and optimization of hybrid energy storage, power electronic converters, and electric propulsion systems.

Heath F. Hofmann (S'90–M'92–SM'16) received the Ph.D. degree in electrical engineering and computer science from the University of California at Berkeley, Berkeley, CA, USA, in 1998.

He is currently a Professor with the University of Michigan, Ann Arbor, MI, USA. He has authored approximately four dozen papers in refereed journals. He currently holds 14 patents. His research interests include power electronics, specializing in the design, simulation, and control of electromechanical systems, adaptive control techniques, energy harvesting, flywheel energy storage systems, electric and hybrid electric vehicles, and finite-element analysis.

Xinfan Lin (M'17) received the B.S. and M.S. degrees in automotive engineering from Tsinghua University, Beijing, China, in 2007 and 2009, respectively, and the Ph.D. degree in mechanical engineering from the University of Michigan, Ann Arbor, MI, USA, in 2014.

He is currently an Assistant Professor with the Department of Mechanical and Aerospace Engineering, University of California, Davis, CA, USA. From 2014 to 2016, he was a Research Engineer with Ford Motor Company, responsible for the development of the battery management system and other EV components and systems. He has published more than 20 peer-reviewed papers and received 2 patents. His research interests include modeling, estimation and control with applications in energy, and automotive systems.

Jing Sun (M'89–SM'00–F'04) received the B.S. and M.S. degrees from the University of Science and Technology of China, Hefei, China, in 1982 and 1984, respectively, and the Ph.D. degree from University of Southern California, Los Angeles, CA, USA, in 1989.

From 1989 to 1993, she was an Assistant Professor with the Electrical and Computer Engineering Department, Wayne State University. She joined Ford Research Laboratory, in 1993, where she worked in the Powertrain Control Systems Department. After spending almost 10 years in industry, she came back to academia and joined the Faculty of the College of Engineering, University of Michigan, Ann Arbor, MI, USA, in 2003, where she is currently the Michael G. Parsons Professor and the Chair with the Department of Naval Architecture and Marine Engineering, with courtesy appointments as a Professor with the Department of Electrical Engineering and Computer Science and the Department of Mechanical Engineering. Her research interests include system and control theory and its applications to marine and automotive propulsion systems. She holds 39 US patents and has coauthored a textbook on *Robust Adaptive Control*.

Dr. Sun a recipient of the 2003 IEEE Control System Technology Award.